Jointly power allocation and phase shift optimization for RIS empowered downlink cellular networks

Phuc Quang Truong[1],*, Tan Do-Duy[1], Van-Ca Phan[1], and Antonino Masaracchia[2]

[1]Faculty of Electrical and Electronics Engineering, Ho Chi Minh City University of Technology and Education
No.1, Vo Van Ngan street, Thu Duc City, Ho Chi Minh City, Vietnam
[2]School of Electronics, Electrical Engineering, and Computer Science, Queen's University Belfast,
Belfast BT7, 1NN, UK

Abstract

Reconfigurable Intelligent Surfaces (RIS) have been highlighted by the research community as a key enabling technology for the enhancement of next-generation wireless network performance, including energy efficiency, spectral efficiency, and network throughput. This paper investigates how RIS-assisted communication can effectively maximize the downlink throughput of a cellular network. Specifically, the paper considers a communication scenario where a single base station serves multiple ground users with the aid of an RIS placed on a building facade. For such a communication scenario, we considered an optimization problem aimed at maximizing the overall downlink throughput by jointly optimizing power allocation at the base station and phase shift of RIS reflecting elements, subject to power consumption and quality-of-service constraints. To address its non-convex nature, the original optimization problem has been divided into two subproblems. The first one, for power control with fixed phase shift values, is a convex problem that can be easily solved. Subsequently, a phase shift searching procedure to solve the non-convex problem of RIS phase shift optimization has been adopted. The results from numerical simulations show that the proposed method outperforms other conventional methods proposed in the literature. In addition, computational complexity analysis has been conducted to prove the low complexity of the proposed method.

1. Introduction

The current generation of wireless communication systems is experiencing a huge increase of connected mobile devices with a corresponding exponential increase of mobile data traffic. According to data analysis and forecasts from the International Telecommunication Union Radiocommunication Sector (ITU-R), this trend will inevitably cause a collapse of the current 5G networks in the near future [2]. Under these perspectives, both industry and academia are actively working towards the development of the new wireless communication network referred as sixth-generation (6G).

This new standard is expected to introduce innovative physical layer technologies that, compared to 5G, will provide increased network capacity, as well as increased reduced latency and better communication reliability [3–5]. Reconfigurable intelligent surface (RIS) is one of these potential technology for 6G [6]. More specifically, RIS is a two-dimensional surface consisting of massive reflecting elements, which are entirely programmable through the usage of appropriate external signals [7]. As result, the adoption of RIS will allow to reflect and redirect the transmitted signal enabling then the possibility to control the signal propagation over the wireless medium. As illustrated in Figure 1, through a RIS-enabled communication scenario it results possible to manipulate and reflect radio signals in order to ensure improved coverage and signal quality, even in

---

*Corresponding author. Email: phuctq@hcmute.edu.vn

challenging environments. Furthermore, compared to massive multiple-input multiple-output (MIMO) technology, RIS represents a more cost-effective and energy-efficient solution. [8]. As result, the adoption of RIS in wireless communication scenarios has gathered significant attention from the research community, who have recognized it as a pivotal enabling technology for 6G due to its immense potential and capabilities [9]. Some of the most relevant works are discussed in the next subsection.

1.1. Related works on RIS

Authors in [10] proved how, compared to amplify-and-forward (AF), a RIS-assisted wireless communication system outperforms in terms of ergodic capacity (EC)and outage probability, and then in terms of lower symbol error rate (SER) and average end-to-end signal-to-noise ratio (SNR). Particularly, the end-to-end wireless channel from source to destination with the assistance of single RIS and multiple RISs was considered, then, the authors derived the close-form expression for OP, and SER in both investigate cases. Likewise, the close-form expression of instantaneous, average end-to-end SNR, and EC of both RIS-assisted RF-relaying wireless system are derived to analyze the performance in case of single RIS and multi-RISs. Additionally, in [11] they considered communication scenario with single antenna at both transmitter and receiver, assisted by a RIS with N reflecting elements. In order to validate the performances of such RIS-asssited scenario, they provided a closed-form expressions the EC upper bound and outage probability approximation under the assumption of mixed Rayleigh and Rician fading channels, which have been validated by using Monte Carlo simulations. This has been further validated in [12], by deriving closed-form expressions for the OP, average SER and average communication rate. Last but not least, the authors also shown how the number of reflecting elements of RIS in single-input single-output (SISO) channel impact on channel diversity. A RIS-aided SISO wireless system with underlying non-orthogonal multiple access (NOMA) communication consisting has been considered in [13]. In this case, OP of the considered system has been derived in closed-form, showing the significant benefit of RIS in enhancing the coverage under the new channel statistics link from BS to cell-edge user devices via RIS with Nakagami-m fading.

In addition to the mathematical models that represents a tangible tool for demonstrating the potential of RIS-assisted communications, several studies have also been conducted with the main aim of optimizing the main variables of the entire communication system and then maximizing the overall system performances.

An optimization framework aimed at maximizing the energy efficiency (EE) of a multiple-input single-output (MISO) RIS-assisted network was proposed in [14]. The proposed optimization framework jointly optimized power allocation at the base station and the phase shift of the RIS to serve multiple users.

Optimization strategies to maximize the weighted sum rate (WSR) of all users have been proposed in [15, 16]. More specifically, authors in [15] considered an RIS-assisted multi-user MISO wireless communication scenario. The considered system consisted in an N-element RIS and one multi-antenna wireless access point providing services to single-antenna users in a quasi-static flat-fading channel environment. In this context, WSR of the network was maximized by jointly optimizing beamforming at the access point and RIS phase-shoft vector. On the other hand, a RIS-aided millimetre-wave (mmWave) massive MIMO was considered in [16]. More specifically, authors considered a system where the direct links between the BS and mobile users are blocked by objects. Under this assumptions, the WSR was maximized by jointly optimizing BS's beamforming matrix and the RIS's phase-shift vector.

An iterative optimization algorithm to maximize the achievable rate of a MIMO system equipped with a RIS have been proposed in [17]. In this case, the proposed algorithm jointly optimized the covariance matrix of the transmitted signal and the phase shift coefficients of RIS elements.

Recently, the possibility of including RIS into unmanned aerial vehicle (UAV) communication scenarios has also gaining attention. Indeed, compared to the conventional BS-based communications, the simultaneous usage of these technologies within the same communication area definitely allows for improving the strength f the signal received by the ground users [18–20]. However, these types of communication scenarios comes with additional variables to optimized in order to maximize the entire system performances, especially in particular where an high quality of connection between UAV and ground users must be guaranteed, such as disaster rescue mission and geography exploration.

Authors in [21] considered a communication scenario with a single UAV, a ground user, and an RIS placade on a building facade. For this communication setup, in order to maximize the average achievable system rate, an optimization framework that jointly optimizes the beamforming vector and the UAV's trajectory was proposed.

In [22], a deep reinforcement learning (DRL) based approach was investigated to maximize the EE of multi-UAV networks. To tackle this problem, a DRL-based method the joint optimization of RIS phase shift optimization and power allocation of UAVs was proposed and validated.

The problem of maximizing the average achievable rate of a RIS-aided UAV network was presented in [23]. To deal with the non-convexity of such problem, the authors proposed to divide the original problem into two sub-problems, i.e., one for passive beamforming optimization and anther for trajectory optimization. Nevertheless, the main focus in [24] was on the maximization of total network throughput through the optimization power allocation and phase shift subject to power consumption constraints and minimum guaranteed quality-of-service at users.

The usage of RIS technology is also gaining attention in the context of Mobile Edge Computing (MEC) scenarios. The usage of RIS within a MEC scenario holds the potential to address the latency requirements envisioned for 6G-enabled MEC services. Especially, in [25] proposed the RIS-aided NOMA network combined with radio frequency energy harvesting and MEC technique. To evaluate the effectiveness of networks parameters to the proposed scheme, the authors considered the optimization problem with two object functions including the probabilities of task offloading and energy transfer efficiency. It is worth to mention that in RIS-aided MEC system, the radio, computing, and wireless environment are considered to optimize [26, 27]. In line with this view, the objective in [26] is to optimize resource allocation including the transmit power and the computing capacity of the RIS-assisted MEC system. It is highlighted that the authors formulated the RIS optimization problem for dependent RIS response profiles over the multi-carrier frequency selective channels. Meanwhile, to overcome the huge challenges of wireless network including the limited coverage and computational capacity, the authors propose the UAV-RIS assisted MEC network in [27]. To exploit the potential of proposed scheme, the authors derived the max-min computation capacity problem through considering the trajectory, computation capacity, beamforming of UAV, and time slot partition, uplink signal detection, and beamforming at RIS as well.

1.2. Motivation and Contributions

This paper represents an extension of the work resented in [1]. In particular, we extend our previous work by jointly optimizing the phase-shift matrix at RIS and power allocation at BS subject to minimum quality-of-service and power constraints, showing how the performances varies as the number of RISs in the area increases. Then, the main contributions of this work can be summarized as follow: The main contributions of this paper are listed as follows:

- We consider a RIS-aided wireless communication scenario were different RISs are deployed in order to provide downlink service to group of users. For such scenario we formulated an optimization problem aimed at maximizing the total network throughput under the power consumption and quality-of-service constraints.

- Due to the non-convexity nature of the proposed problem, we divided into two sub-problems, for which an iterative frameworks is proposed. Such framework summarized in Algorithm 1 and Algorithm 2, was based on the usage of effective approximations, logarithm inequalities for relaxation.

- Finally, we investigated how the proposed joint optimization method outperform in maximizing total network throughput and the worst case mobile unit throughput compared to conventional methods.

The rest of the paper is organized as follows. System model and the problem formulation are provided in Section 2.1. Section 3, illustrates the joint power allocation and phase shift optimization, and how it is divided into two subproblems including power control coefficients optimization and RIS phase shift optimization, respectively. Simulation and performance evaluations results are discussed in Section 4. Finally, the paper is concluded Section 5.

Table 1. Notations

Symbol	Definition
H_0, H_m	BS and the RIS height, respectively.
$\boldsymbol{\Phi}_m$	Phase shift matrix of the m-th RIS
H	Hermitian conjugate operation
$\mathbf{h}_{0,m} \in \mathbb{C}^{N \times 1}$	Channel matrix between the BS and the m-th RIS
$\mathbf{h}_{m,k}^H \in \mathbb{C}^{1 \times N}$	Channel matrix between the m-th RIS to the (m, k)-th MU
$p_{m,k}$	Transmission power of BS to the (m,k)-th MU
$\omega_k \sim \mathcal{CN}(0, \sigma_k^2)$	AWGN at the (m,k)-th MU
α	Path loss exponent
$\mathbf{g}_{m,k} \in \mathbb{C}$	Cascaded channel matrix of the link BS–(m,k)th MU
$p_{m,k}$	Transmission power of the BS to the (m,k)-th MU
η^{LoS}, η^{NLoS}	Average additional losses of LoS and NLoS

2. System Model and Problem Formulation

In this section, we investigate the signal model for downlink multi-user SISO cellular network, then we formulate an optimization problem for maximizing the total network throughput by jointly optimal allocation of of transmit power at BS and phase shift of RIS.
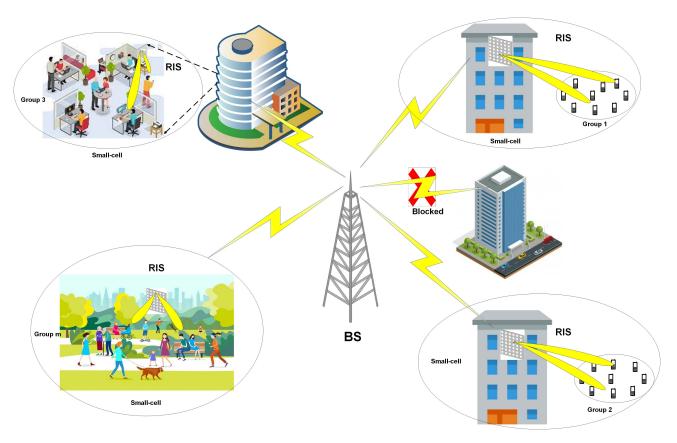
Figure 1. RIS–assisted downlink cellular communications.

2.1. System Model

Due to the objects obstructing the communication link, the mobile users (MUs) in cellular network either receive low quality signal or not signal at all from the BS. To tackle this problem, we propose the system model in Fig. 1, particularly we focus on enhancing the total network throughput of the multi-user cellular network with the assistance of RISs. More specifically, how illustrated in Fig. 1, we consider a single antenna BS serving a set of $\mathcal{M} = \{1, ..., M\}$ small cells, each of them containing different numbers of MUs, which are supposed to be uniformly distributed within the whole coverage area. All these aures are indicated as $\mathcal{K} = \{1, ..., K\}$. In order to solve the issue by blockage effect from buildings and other obstacles, it is supposed that different N-element RISs are placed on the facade of different buildings building, each of them used to cover a specific small cell. The number of MUs covered by the m-th cell are indicated as $\mathcal{K}_m = \{1, ..., K_m\}$ for $m \in \mathcal{M}$, while the k-th user within the m-th group as (m, k)

2.2. Communication Model

Within the considered communication scenario, the 3D Cartesian coordinates of the BS, the RISs and of the generic MU are indicated as (x_0, y_0, H_0), (x_m, y_m, H_m), $m \in \mathcal{M}$ and $(x_k, y_k, 0)$, $k \in \mathcal{K}$, with H_0 and H_m being the z-coordinate, i.e., height the BS and the RIS altitude, respectively. We assume that there exists a direct communication between BS and the m-th RIS. Then, as also assumed in [28, 29], such communication link follow the free-space path loss model:

$$\beta_{0,m} = \beta_0 l_{0,m}^{-2}, \ m = 1, ..., M, \tag{1}$$

with β_0 being the channel gain at reference position, and $l_{0,m}$ the distance between the BS and the m-th RIS calculated as:

$$l_{0,m} = \sqrt{d_{0,m}^2 + (H_0 - H_m)^2}, \tag{2}$$

with $d_{0,m} = \sqrt{(x_0 - x_m)^2 + (y_0 - y_m)^2}$.

On the other hand, since the channel from the RIS to the MUs is usually affected by shadowing and blockage, a non-LoS (NLoS) model is applied. In this case then, the channel from the m-th RIS to the (m, k)-th MU is modelled as [30]

$$\beta_{m,k} = PL_{m,k} + \eta^{LoS} P_{m,k}^{LoS} + \eta^{NLoS} P_{m,k}^{NLoS}$$
$$= 10\alpha \log\left(\sqrt{d_{m,k}^2 + H_m^2}\right) + AP_{m,k}^{LoS} + B, \tag{3}$$

where η^{LoS} and η^{NLoS} are the average additional losses for LoS and NLoS, respectively, $A = \eta^{LoS} - \eta^{NLoS}$ and $B = 10\alpha \log(\frac{4\pi l_{m,k}}{\lambda_c}) + \eta^{NLoS}$. The path loss is given as follows:

$$PL_{m,k} = 10 \log(\frac{4\pi l_{m,k}}{\lambda_c})^{\alpha}, \ m = 1, ..., M, \quad (4)$$

where $\lambda_c = c/f_c$ is the wavelength of the carrier at frequency f_c epressed in Hz, while $\alpha \geq 2$ is the path loss exponent. As regards the probability of LoS and NLoS, they are modelled by [31]:

$$P_{m,k}^{LoS} = \frac{1}{1 + a \exp\left[-b\left(\arctan\left(\frac{H_m}{d_{m,k}}\right) - a\right)\right]}, \quad (5)$$

$$P_{m,k}^{NLoS} = 1 - P_{m,k}^{LoS}, \quad (6)$$

whit a and b representing environmental constraints.

Finally, the phase shift matrix at the m-th RIS is expressed as:

$$\boldsymbol{\Phi}_m = diag[\phi_{1m}, \phi_{2m}, ..., \phi_{Nm}], m \in \mathcal{M} \quad (7)$$

where $diag(\mathbf{a})$ denotes a diagonal matrix having the element of vector $\mathbf{a}$ along its diagonal. More specifically, each coefficient is modelled as $\phi_{nm} = \alpha_{nm}e^{j\theta_{nm}}$ with $\alpha_{nm} \in [0, 1]$ and $\theta_{nm} \in [0, 2\pi]$ ($\forall n = 1, 2, ..., N, \ m \in \mathcal{M}$) indicating the amplitude and phase shift of received by the signal from the n-th reflecting element. It is worth to mention that we assume $\alpha_{nm} = 1$ [32]. In order to take into account the effect of the small scale fading coefficients, we assume that for both BS to m-th RIS, and m-th RIS to the (m, k)-th MU channels, the small-scale fading contributions are modelled as independent and identically distributed random variables with zero mean and unit variance, respectively indicated as $\hat{h}_{0,m} \in \mathbb{C}^{N \times 1}$ and $\hat{h}_{m,k}^H \in \mathbb{C}^{1 \times N}$. We also also use $\mathbf{h}_{0,m} \in \mathbb{C}^{N \times 1}$ and $\mathbf{h}_{m,k}^H \in \mathbb{C}^{1 \times N}$ to indicate the matrices containing the channel coefficients between the BS and the m-th RIS and the m-th RIS to the (m, k)-th MU in the m-th group, respectively. As result the total channel coefficient from the BS to the (m, k)-th MU through the m-th RIS can be expressed as [33]:

$$\mathbf{g}_{m,k} = \mathbf{h}_{m,k}^H \boldsymbol{\Phi}_m \mathbf{h}_{0,m}, \ m \in \mathcal{M}, \ k \in \mathcal{K}_m, \quad (8)$$

where $\mathbf{h}_{0,m} = \sqrt{\beta_{0,m}}\hat{h}_{0,m}$ and $\mathbf{h}_{m,k}^H = \sqrt{\beta_{m,k}}\hat{h}_{m,k}^H$.

2.3. Signal Model

As illustrated in Figure 1, we have considered a downlink communication scenario where a signal from a BS is trnasmitted to K single antenna MUs with the support of RISs deployed on buildings facade to help in improving the BS-MUs communication link. Supposing

that the communications are performed through the Time Division Multiple Access (TDMA) scheme, the signal at the k-th MU in the m-th group can be expressed as:

$$y_{m,k} = \sqrt{p_{m,k}}\mathbf{g}_{m,k}x_{m,k} + \omega_k, \ m \in \mathcal{M}, \ k \in \mathcal{K}_m, \quad (9)$$

in which $p_{m,k}$ denotes the transmission power allocated by the BS to the (m, k)-th MU, $x_{m,k}$ with $\|x_{m,k}\|^2 \leq 1$ is the informative message, $\omega_k \sim \mathcal{CN}(0, \sigma_k^2)$ is the Additive White Gaussian Noise (AWGN).

indicating with $\boldsymbol{p}_0 = [\boldsymbol{p}_{0,m}]_{m=1}^M$, where $\boldsymbol{p}_{0,m} = [p_{m,k}]_{k=1}^{K_m}$ power control coefficients used at the BS, and with $\boldsymbol{\Phi}_M = [\boldsymbol{\Phi}_m]_{m=1}^M$ the phase shifts coefficients of RISs, the SNR at the (m, k)-th MU be formulated as

$$\gamma_{m,k}\left(p_{m,k}, \boldsymbol{\Phi}_m\right) = \frac{p_{m,k}\left|\mathbf{g}_{m,k}\right|^2}{\sigma_k^2}. \quad (10)$$

Then, the throughput of the (m, k)-th MU, expressed in bit per second per Hertz (bps/Hz) can be expressed using the Shannon formula for the channel capacity:

$$R_{m,k}\left(p_{m,k}, \boldsymbol{\Phi}_m\right) = \log_2\left(1 + \gamma_{m,k}\left(p_{m,k}, \boldsymbol{\Phi}_m\right)\right) \quad (11)$$

Finally, the total throughput of all MUs in the considered network can be formulated as

$$R_{total}\left(\boldsymbol{p}_0, \boldsymbol{\Phi}_M\right) = \sum_{m=1}^M \sum_{k=1}^{K_m} R_{m,k}\left(p_{m,k}, \boldsymbol{\Phi}_m\right). \quad (12)$$

2.4. Problem Formulation

As already mentioned before, we aim at jointly optimizing the power control coefficients ($\boldsymbol{p}_0$) at the BS and the phase shift ($\boldsymbol{\Phi}_M$) of the RISs, in order to maximize the total downlink network throughput, under power consumption and QoS constraints. To this end, we formulated the following optimization problem:

$$\max_{\boldsymbol{p}_0, \boldsymbol{\Phi}_M} R_{total}\left(\boldsymbol{p}_0, \boldsymbol{\Phi}_M\right) \quad (13a)$$

$$\text{s.t.} \quad \sum_{m=1}^M \sum_{k=1}^{K_m} p_{m,k} \leq P_0^{\max}, \ m \in \mathcal{M}, \ k \in \mathcal{K}_m, \quad (13b)$$

$$R_{m,k}\left(p_{m,k}, \boldsymbol{\Phi}_m\right) \geq \bar{r}_{m,k}, \ m \in \mathcal{M}, \ k \in \mathcal{K}_m, \quad (13c)$$

$$0 \leq \theta_{nm} \leq 2\pi, \forall n = 1, 2, ..., N, \ m \in \mathcal{M}, \quad (13d)$$

where the constraint (13b) represents the total power consumption constraint at the BS. On the other hand, constraints (13c) and (13d) accounts for the individual QoS requirement at the (m, k)-th MU and lower and upper bounds of the phase shifts of RIS elements, respectively.

3. Proposed Optimization Framework

In order to deal with the non-convexity of problem (13) and its related constraints, we proposed an algorithm that iteratively optimize the power control coefficients at the BS and the phase shifts of RIS reflecting elements. The main components of this algortihm are explained in the following subsections.

3.1. Optimization of Power Control Coefficients

At this stage we assume that Φ_M is fixed, then (13) obtaining then the following optimization problem for the power coefficients:

$$\max_{\boldsymbol{p}_0} R_{total}\left(\boldsymbol{p}_0\right) \tag{14a}$$

$$\text{s.t.} \quad (13b), (13c). \tag{14b}$$

This problem is solved by an effective approximation obtained by using logarithm inequalities [34, 35] based on the property that the convex function $f(z) = \log_2(1 + \frac{1}{z}) \geq \hat{f}(z)$, with

$$\hat{f}(z) = \log_2\left(1 + \frac{1}{\bar{z}}\right) + \frac{1}{1 + \bar{z}} - \frac{z}{(1 + \bar{z})\bar{z}}, \tag{15}$$

$\forall z > 0, \bar{z} > 0$. Then, the throughput expression can be rewritten as:

$$R_{m,k}\left(p_{m,k}\right) \geq \hat{R}_{m,k}^{(iter)}\left(p_{m,k}\right), \forall k \in \mathcal{K}_m, \forall m \in \mathcal{M}, \tag{16}$$

where

$$z = \frac{\sigma_k^2}{p_{m,k}\left|g_{m,k}\right|^2}, \quad \bar{z} = z^{(iter)} = \frac{\sigma_k^2}{p_{m,k}^{(iter)}\left|g_{m,k}\right|^2},$$

$$\hat{R}_{m,k}^{(iter)}\left(p_{m,k}\right) = \log_2\left(1 + \frac{1}{\bar{z}}\right) + \frac{1}{1 + \bar{z}} - \frac{z}{(1 + \bar{z})\bar{z}}. \tag{17}$$

Then, the optimization problem (14) at the i-th iteration can be rewritten as:

$$\max_{\boldsymbol{p}_0} \hat{R}_{total}^{(iter)}\left(\boldsymbol{p}_0\right) \tag{18a}$$

$$\text{s.t.} \quad (13b), \tag{18b}$$

$$\hat{R}_{m,k}^{(iter)}\left(\boldsymbol{p}_0\right) \geq \bar{r}_{m,k}, \ m \in \mathcal{M}, \ k \in \mathcal{K}_m, \tag{18c}$$

where $\hat{R}_{total}^{(\kappa)}\left(\boldsymbol{p}_0\right) = \sum_{m=1}^{M} \sum_{k=1}^{K_m} \hat{R}_{m,k}^{(\kappa)}\left(p_{m,k}\right)$.
It is noticed that (18) is convex. Thus, it can be solved efficiently by using standard software, such as CVX tools[36]. The proposed iterative power allocation procedure to solve the problem (18) to provide the optimal power control coefficients $(\boldsymbol{p}_0^*)$ is summarized in the Algorithm 1, where the maximum number of iterations is $Iter_{max} = 20$.

Algorithm 1 Power allocation procedure

1: **Initialize**:
2:     Let the iteration value $iter = 0$ and $Iter_{max} = 20$
3:     Let the feasible point for Φ_M, and the tolerance $\xi = 10^{-3}$
4: **while** (The convergence is not reach or $iter \leqslant I_{max}$)

5:     Solve (18) to find $(\boldsymbol{p}_0^{(i+1)})$ using CVX tool
6:     Update $iter = iter + 1$
7: **end while**
8: **Output**: the optimal power control coefficients $\boldsymbol{p}_0^*$

3.2. Phase Shift Optimization

Similarly, we assume that power control coefficients $\boldsymbol{p}_0$ is fixed, thus the problem (13) can be rewritten as follows:

$$\max_{\Phi_M} R_{total}\left(\Phi_M\right) \tag{19a}$$

$$\text{s.t.} \quad (13c), (13d). \tag{19b}$$

In this problem we introduce the notation for the cascaded channel $\boldsymbol{h}_{m,k}^H \Phi_m \boldsymbol{h}_{0,m} = v_m^H \chi_{m,k}$ where $v_m = [v_m^1, ..., v_m^N]^H$ with $v_m^n = e^{j\theta_{nm}}$ ($\forall n = 1, 2, ..., N$), $\chi_{m,k} = diag(\boldsymbol{h}_{m,k}^H)\boldsymbol{h}_{0,m}$, and $\rho_k = P_0/\sigma_k^2$. Supposing $|v_m^n|^2 = 1$, the (13d) constraints becomes the unit-modulus constraint [37]. Then, the problem (19) is equivalent to the following:

$$\max_{v_m, \ m\in\mathcal{M}} \sum_{m=1}^{M} \sum_{k=1}^{K_m} \log_2\left(1 + \rho_k v_m^H \chi_{m,k} \chi_{m,k}^H v_m\right) \tag{20a}$$

$$\text{s.t.} \quad v_m^H \chi_{m,k} \chi_{m,k}^H v_m \geq \left(2^{\bar{r}_{m,k}} - 1\right)/\rho_k, \tag{20b}$$

$$|v_m^n|^2 = 1, \forall n = 1, 2, ..., N, \ m \in \mathcal{M}. \tag{20c}$$

Since (20) is still non-convex we used a relaxation method in order to obtain a convex version of this optimization problem. In particular, we first denote $\mathbf{X}_{m,k} = \chi_{m,k}\chi_{m,k}^H$ and $v_m^H \mathbf{X}_{m,k} v_m = tr\left(\mathbf{X}_{m,k} v_m v_m^H\right) = tr\left(\mathbf{X}_{m,k} \Upsilon_m\right)$ where $\Upsilon_m = v_m v_m^H$ satisfies the condition $\Upsilon_m \geq \mathbf{0}$ and rank(Υ_m)=1, $\forall m \in \mathcal{M}$. This allowed us to relax the rank-one constraint of (20c) [38]. Finally, (20) can be rewritten as:

$$\max_{v_m, \ m\in\mathcal{M}} \sum_{m=1}^{M} \sum_{k=1}^{K_m} \log_2\left(1 + \rho_k tr\left(\mathbf{X}_{m,k} \Upsilon_m\right)\right) \tag{21a}$$

$$\text{s.t.} \quad tr\left(\mathbf{X}_{m,k} \Upsilon_m\right) \geq \left(2^{\bar{r}_{m,k}} - 1\right)/\rho_k, \tag{21b}$$

$$\Upsilon_{m(n,n)} = 1, \forall n = 1, 2, ..., N, \ m \in \mathcal{M}, \tag{21c}$$

$$\Upsilon_m \geq \mathbf{0}. \tag{21d}$$

Problem (21) is a convex semidefinite program (SDP) [37], which can be efficiently solved by using

CVX tool. Algorithm 2 illustrate the proposed Block Coordinate Descendent (BCD) method employed to find the optimal phase shift ($\mathbf{\Phi}_M^*$).

Algorithm 2 Phase shift searching procedure

1: **Initialize:**
2:     Let the iteration value $iter = 0$ and $Iter_{max} = 20$
3:     Let the feasible point for $\boldsymbol{p}_0$, $\xi = 10^{-3}$, and $\boldsymbol{f}_{m,k}^{(0)}$
4: **while** (The convergence is not reach or $iter \leqslant I_{max}$)

5:     **for** m in range $[1:M]$
6:         Solve (21) to find ($\mathbf{\Phi}_M^{(iter+1)}$) using CVX tool
7:         Update $f_{m,k}^{(iter+1)}$
8:     **end for**
9:     Update $iter = iter + 1$
10: **end while**
11: **Output**: The optimal phase shift $\mathbf{\Phi}_M^*$

Then, the intractable optimization problem in (13) is solved by combining the Algorithm 1 power allocation optimization and Algorithm 2 RIS phase shift optimization.

4. Simulation Results

Table 2. Simulation Parameters

Parameter	Value
Radius of BS's coverage circle	500m
Radius of expanded deployment	1500m
BS's location	(0,0,30)m
White noise power density	–130 dBm/Hz
QoS threshold	1 bps/Hz
Tolerance for convergence of algorithm	$\xi = 10^{-3}$
Bandwidth	10MHz
BS transmit power	[43:46]dBm
Number of users in small cell	[20, 30]
Number of RISs	[4, 8, 12, 20]
Number of reflecting elements	[100, 150, 200, 250, 300]

In this section, we illustrate the performances of our proposed optimization method obtained through numerical simulation carried out using Matlab. To perform the simulation, we use the personal computer with CPU Intel(R) Core(TM) i7-9700 CPU @ 3.00GHz and 16GB memory. Simulation parameters are summarized in Table 2. As regards the channel modelling we considered the same settings adopted in [34, 39]. The performances of our proposed method, indicated as **(OOP)**, have been compared with the performances achieved by oter conventional methods such as Optimal power allocation with Random phase shift **(ORP)**, and Equal power allocation with Optimal phase shift
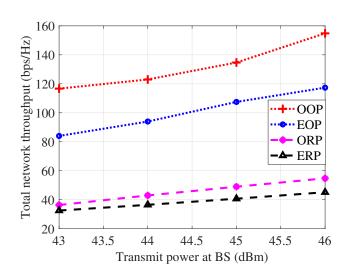

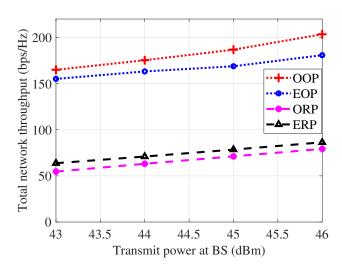**Figure 2.** Total network throughput versus transmission power at BS with $M = 4$, $K = 20$, $N = 200$.

Figure 3. Total throughput versus transmission power at BS with $M = 8$, $K = 30$, $N = 200$.

(EOP) demonstrate the results in case of either without optimizing power allocation or without phase shift optimization, respectively. Additional, the Equal power allocation - Random phase shift **(ERP)** has also been considered, which is the one not optimizing neither power allocation nor phase shift coefficients.

4.1. The total network throughput

To demonstrate the outperform of jointly optimization problem, we show the results in difference scenarios obtained by changing maximum transmit power, number of RIS, and number of reflecting elements per RIS. To take into account the effect of both number of RIS and number of MU in each group of user, Figure 2 illustrates how the total network throughput
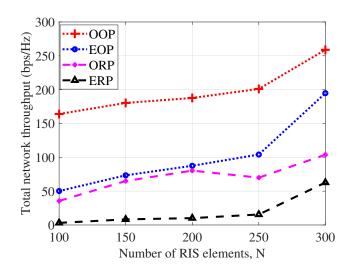
Figure 4. Total throughput versus number of reflecting elements ($M = 8$, $K = 30$, $P_0^{\max} = 46$ dBm).

Figure 5. Total network throughput of the proposed method jointly optimization with different number of RISs ($M = 4$, $M = 12$, $M = 20$).

varies when he number of RISs and the number of UEs are $M = 4$ and $K = 20$, respectively. Similarly, Figure 3 illustrates the case when $M = 8$ and $K = 30$. In both cases, the number of reflecting elements per RIS is fixed to $N = 200$. As a general trend, one can easily note how the total network throughput increases as the transmit power at the BS increases too. In addition, from these two figures we can also observe how the gap between the proposed method (**OOP**) and the **ERP** becomes bigger as the transmit power goes up. Last but not least, the total network throughput also increases number of RISs in the scenario. We can then state that the consider method, where the optimal phase shift is obtained through Algorithm 2, result to be more efficient than the others in all scenarios in Figure 2 and Figure 3. It is obvious the **OOP** achieved approximately four times higher than the **ERP** without optimization at $P_0^{\max} = 45$ dBm with $M = 30$, $K = 30$, and $N = 200$ in Figure 3.

We also illustrate how the total network throughput varies with different number of reflecting elements per RIS, which in Figure 4 vary from 100 to 300 while $M = 8$, $K = 30$, and $P_0^{\max} = 46$ dBm. In this case, it can also be observed how to an increase of number of reflecting elements corresponds an increase of the total network throughput. In particular, as exptected, it can be noted how the total network throughput achieved though the **OOP** is significantly larger than others resource allocation schemes. Particulary, it can achieve approximately a four times higher throughput when compared with the **ERP**. Finally, the results in Figure 5 demonstrate the total network throughput of obtained by the proposed method by varying the number of RIS, i.e., $M = 4$, $M = 12$, and $M = 20$, respectively. Also in this case, it can be observed how the total network
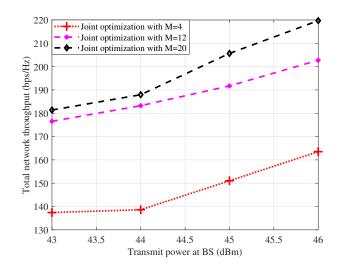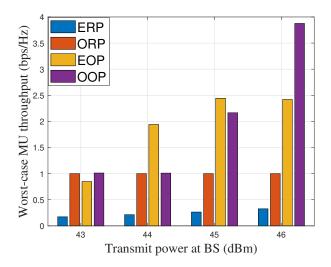

Figure 6. Worst-case MU throughput versus transmit power at BS ($M = 8$, $K = 30$, $N = 200$).

throughput increases significantly when the number of RIS rises from $M = 4$ to $M = 20$. Particularly, the gap of throughput between $M = 4$ to $M = 20$ changes steeply when the transmit power increase from $44dBm$ to $46dBm$, i.e., approximately $56bps/Hz$ at peak transmit power $46dBm$.

4.2. The worst-case MU throughput

In this part, we consider the total network throughput of the worst-case MU in order to prove the proposed method outperform when compared with conventional scheme also in this case.

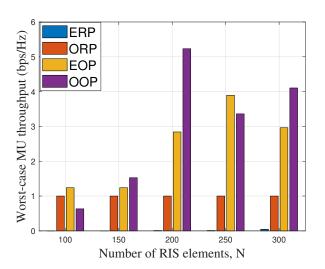As expected, the result in Figure 6 demonstrates the superiority of the proposed method (**OOP**) compared

Figure 7. Worst–case MU throughput versus number of RIS elements N ($M = 20$, $K = 30$, $P_0^{\max} = 46dBm$).
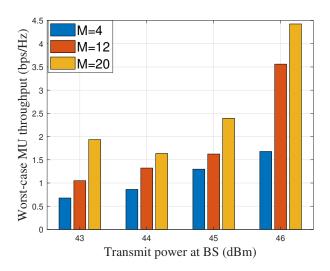

Figure 8. Worst–case MU throughput of the proposed method jointly optimization with different number of RISs ($M = 4$, $M = 12$, $M = 20$).

to the conventional schemes including **OPH**, **EOP**, and **ERP**, respectively, in case of worst-case MU throughput when the values are fixed at $M = 8$, $K = 30$, and $N = 200$. At the onset, it is clear that the worst MU throughput of **OOP** is equal to 1 bps/Hz at $P_0^{\max} = 43dBm$, and $P_0^{\max} = 44dBm$, while at $P_0^{\max} = 45dBm$, and $P_0^{\max} = 46dBm$ are higher and reach the peak value approximately double at $P_0^{\max} = 46dBm$. Likewise, **ORP** achieves a 1 bps/Hz thoguhput when the transmit power of BS grows up from $P_0^{\max} = 43dBm$ to $P_0^{\max} = 46dBm$, meanwhile the worst MU throughput of **EOP** increase when the transmit power increases. However, without optimization **ERP**, the worst MU throughput is

less than 0.5 bps/Hz, so it is unsatisfied the individual QoS constraints in (13c).

On the other hand, to prove the effect of the number of reflecting element per RIS, in Figure 7, we plot the worst-case MU throughput by fixing $P_0^{\max} = 46dBm$), $M = 20$, $K = 30$, while the number of reflecting elements ranges from 100 to 300. In this case , it can be noticed that the throughput achieved by the worst-cse MU mostly satysfies the individual QoS constraint expressed in (13c) with the value higher than $1bps/Hz$, except when the minimum considered transmit power $P_0^{\max} = 43dBm$ is considered. Conversely, it is obvious the when no optimization is applied, i.e., **ERP**, the MU throughput of the worst-case MU is nearly equal to zero even if the number of reflecting element increases. On the other hand, Figure 8 shows the worst-case MU throughput achieved by varying the number of RIS ($M = 4$, $M = 12$, $M = 20$), while the number of reflecting element is fixed to $N = 200$, and the number of user in each small cell is fixed to $K = 30$. It can be seen from this figure that in the majority of cases the MU throughput of the proposed method is mostly greater than 1 bps/Hz, as well as how the perceived throughput increases when the number of RISs and the transmit power of BS increase too. Last but not least, the MU throughput at $M = 20$ is approximately 2.5 times higher than MU throughput at $M = 12$ when the transmit power is set at $P_0^{\max} = 43dBm$.

5. Conclusions and Future Directions

In this paper, we have investigated how the integration of RIS can improve the network performances of SISO downlink cellular wireless networks. Specifically, our focus has been on optimizing the total network throughput under the constraints of maximum transmit power at the BS and QoS requirements of users. To address this challenge, we formulated a related optimization problem, for which we have introduced an iterative algorithm that jointly optimizes the power allocation and phase shift of RISs. The numerical results outlined the efficacy of our proposed system when compared to other conventional resource allocation schemes. In particular it has been illustrated how the total network throughput can be highly maximized when both power allocation and phase shift are optimized. Furthermore, even in worst-case MU scenarios throughput, the proposed methods demonstrates superior performance when power allocation and phase shift coefficients are jointly optimized. As future research direction, we will extend this work by considering multiple antennas BS, and then introducing the active beamforming at BS into the optimization problem.

Acknowledgements

References

[1] Truong PQ, Van CP. Reconfigurable Intelligent Surfaces for Downlink Cellular Networks. In: Vo NS, Vien QT, Ha DB, editors. Industrial Networks and Intelligent Systems. Cham: Springer International Publishing; 2022. p. 20-32.

[2] ITU-R. IMT Traffic Estimates for the Years 2020 to 2030; 2015.

[3] Bui TT, Nguyen LD, Kha HH, Vo NS, Duong TQ. Joint Clustering and Resource Allocation Optimization in Ultra-Dense Networks with Multiple Drones as Small Cells Using Game Theory. Sensors. 2023;23(8). Available from: https://www.mdpi.com/1424-8220/23/8/3899.

[4] Wikström G, Peisa J, Rugeland P, Johansson N, Parkvall S, Girnyk M, et al. Challenges and Technologies for 6G. In: 2020 2nd 6G Wireless Summit (6G SUMMIT); 2020. p. 1-5.

[5] Wang CX, Huang J, Wang H, Gao X, You X, Hao Y. 6G Wireless Channel Measurements and Models: Trends and Challenges. IEEE Vehicular Technology Magazine. 2020;15(4):22-32.

[6] Gong S, Lu X, Hoang DT, Niyato D, Shu L, Kim DI, et al. Toward Smart Wireless Communications via Intelligent Reflecting Surfaces: A Contemporary Survey. IEEE Communications Surveys Tutorials. 2020;22(4):2283-314.

[7] Nguyen KK, Masaracchia A, Yin C. Deep Reinforcement Learning for Intelligent Reflecting Surface-assisted D2D Communications. EAI Endorsed Transactions on Industrial Networks and Intelligent Systems. 2023 Jan;10(1):e1. Available from: https://publications.eai.eu/index.php/inis/article/view/2864.

[8] Strinati EC, Alexandropoulos GC, Wymeersch H, Denis B, Sciancalepore V, D'Errico R, et al. Reconfigurable, Intelligent, and Sustainable Wireless Environments for 6G Smart Connectivity. IEEE Commun Mag. 2021 Oct;59(10):99-105.

[9] Alghamdi R, Alhadrami R, Alhothali D, Almorad H, Faisal A, Helal S, et al. Intelligent Surfaces for 6G Wireless Networks: A Survey of Optimization and Performance Analysis Techniques. IEEE Access. 2020;8:202795-818.

[10] Boulogeorgos AAA, Alexiou A. Performance Analysis of Reconfigurable Intelligent Surface-Assisted Wireless Systems and Comparison With Relaying. IEEE Access. 2020;8:94463-83.

[11] Tao Q, Wang J, Zhong C. Performance Analysis of Intelligent Reflecting Surface Aided Communication Systems. IEEE Communications Letters. 2020;24(11):2464-8.

[12] Kudathanthirige D, Gunasinghe D, Amarasuriya G. Performance Analysis of Intelligent Reflective Surfaces for Wireless Communication. In: ICC 2020 - 2020 IEEE International Conference on Communications (ICC); 2020. p. 1-6.

[13] Cheng Y, Li KH, Liu Y, Teh KC. Outage Performance of Downlink IRS-Assisted NOMA Systems. In: GLOBECOM 2020 - 2020 IEEE Global Communications Conference; 2020. p. 1-6.

[14] Huang C, Zappone A, Alexandropoulos GC, Debbah M, Yuen C. Reconfigurable Intelligent Surfaces for Energy Efficiency in Wireless Communication. IEEE Transactions on Wireless Communications. 2019;18(8):4157-70.

[15] Guo H, Liang YC, Chen J, Larsson EG. Weighted Sum-Rate Maximization for Reconfigurable Intelligent Surface Aided Wireless Networks. IEEE Transactions on Wireless Communications. 2020;19(5):3064-76.

[16] Cao Y, Lv T, Ni W. Intelligent Reflecting Surface Aided Multi-User mmWave Communications for Coverage Enhancement. In: 2020 IEEE 31st Annual International Symposium on Personal, Indoor and Mobile Radio Communications; 2020. p. 1-6.

[17] Perović NS, Tran LN, Di Renzo M, Flanagan MF. Achievable Rate Optimization for MIMO Systems With Reconfigurable Intelligent Surfaces. IEEE Transactions on Wireless Communications. 2021;20(6):3865-82.

[18] Li Y, Yin C, Do-Duy T, Masaracchia A, Duong TQ. Aerial Reconfigurable Intelligent Surface-Enabled URLLC UAV Systems. IEEE Access. 2021;9:140248-57.

[19] Masaracchia A, Li Y, Nguyen KK, Yin C, Khosravirad SR, Costa DBD, et al. UAV-Enabled Ultra-Reliable Low-Latency Communications for 6G: A Comprehensive Survey. IEEE Access. 2021;9:137338-52.

[20] Nguyen KK, Masaracchia A, Sharma V, Poor HV, Duong TQ. RIS-Assisted UAV Communications for IoT With Wireless Power Transfer Using Deep Reinforcement Learning. IEEE J Sel Topics Signal Process. 2022;16(5):1086-96.

[21] Li S, Duo B, Yuan X, Liang YC, Di Renzo M. Reconfigurable Intelligent Surface Assisted UAV Communication: Joint Trajectory Design and Passive Beamforming. IEEE Wireless Communications Letters. 2020;9(5):716-20.

[22] Nguyen KK, Khosravirad SR, da Costa DB, Nguyen LD, Duong TQ. Reconfigurable Intelligent Surface-Assisted Multi-UAV Networks: Efficient Resource Allocation With Deep Reinforcement Learning. IEEE Journal of Selected Topics in Signal Processing. 2022;16(3):358-68.

[23] Ren H, Zhang Z, Peng Z, Li L, Pan C. Energy Minimization in RIS-Assisted UAV-Enabled Wireless Power Transfer Systems. IEEE Internet of Things Journal. 2023;10(7):5794-809.

[24] Nguyen MHT, Garcia-Palacios E, Do-Duy T, Dobre OA, Duong TQ. UAV-Aided Aerial Reconfigurable Intelligent Surface Communications With Massive MIMO System. IEEE Transactions on Cognitive Communications and Networking. 2022;8(4):1828-38.

[25] Ha DB, Truong VT, Lee Y. Intelligent Reflecting Surface assisted RF Energy Harvesting Mobile Edge Computing NOMA Networks: Performance Analysis and Optimization. EAI Endorsed Transactions on Industrial Networks and Intelligent Systems. 2022 Aug;9(32):e5. Available from: https://publications.eai.eu/index.php/inis/article/view/1376.

[26] Merluzzi M, Costanzo F, Katsanos KD, Alexandropoulos GC, Di Lorenzo P. Power Minimizing MEC Offloading

with QoS Constraints over RIS-Empowered Communications. In: GLOBECOM 2022 - 2022 IEEE Global Communications Conference; 2022. p. 5457-62.

[27] Xu Y, Zhang T, Liu Y, Yang D, Xiao L, Tao M. Computation Capacity Enhancement by Joint UAV and RIS Design in IoT. IEEE Internet of Things Journal. 2022;9(20):20590-603.

[28] Nguyen MN, Nguyen LD, Duong TQ, Tuan HD. Real-Time Optimal Resource Allocation for Embedded UAV Communication Systems. IEEE Wireless Communications Letters. 2019;8(1):225-8.

[29] Bor-Yaliniz RI, El-Keyi A, Yanikomeroglu H. Efficient 3-D placement of an aerial base station in next generation cellular networks. In: IEEE ICC; 2016. p. 1-5.

[30] Mozaffari M, Saad W, Bennis M, Debbah M. Efficient Deployment of Multiple Unmanned Aerial Vehicles for Optimal Wireless Coverage. IEEE Commun Lett. 2016 Aug;20:1647-50.

[31] Al-Hourani A, Kandeepan S, Lardner S. Optimal LAP Altitude for Maximum Coverage. IEEE Wireless Communications Letters. 2014;3(6):569-72.

[32] Xie X, Fang F, Ding Z. Joint Optimization of Beamforming, Phase-Shifting and Power Allocation in a Multi-cluster IRS-NOMA Network. IEEE Trans Veh Technol. 2021:1-1.

[33] Wu Q, Zhang R. Beamforming Optimization for Wireless Network Aided by Intelligent Reflecting Surface With Discrete Phase Shifts. IEEE Trans Commun. 2020;68(3):1838-51.

[34] Nguyen LD, Tuan HD, Duong TQ, Dobre OA, Poor HV. Downlink Beamforming for Energy-Efficient Heterogeneous Networks With Massive MIMO and Small Cells. IEEE Transactions on Wireless Communications. 2018;17(5):3386-400.

[35] Duong T. Real Time Convex Optimisation for 5G Networks and Beyond. Institution of Engineering and Technology (IET); 2021.

[36] Grant M, Boyd S. CVX: MATLAB Software for Disciplined Convex Programming, version 2.1; 2014. http://cvxr.com/cvx.

[37] Wu Q, Zhang R. Intelligent Reflecting Surface Enhanced Wireless Network via Joint Active and Passive Beamforming. IEEE Trans Wireless Commun. 2019;18(11):5394-409.

[38] Yu H, Tuan HD, Nasir AA, Duong TQ, Poor HV. Joint Design of Reconfigurable Intelligent Surfaces and Transmit Beamforming Under Proper and Improper Gaussian Signaling. IEEE Journal on Selected Areas in Communications. 2020;38(11):2589-603.

[39] Do-Duy T, Nguyen LD, Duong TQ, Khosravirad S, Claussen H. Joint Optimisation of Real-time Deployment and Resource Allocation for UAV-Aided Disaster Emergency Communications. IEEE Journal on Selected Areas in Communications. 2021:1-1.